

Balancing local frequency content in seismic data using non-stationary smoothing

Sarah Yvonne Greer

ABSTRACT

Seismic data can experience non-stationary frequency variations caused by attenuation. This problem is encountered when matching multiple data sets, such as in multicomponent image registration, because signals with differing frequency content are hard to correlate. In this chapter, we introduce two methods for balancing frequency content between data sets while taking into account non-stationary frequency variations. Both methods involve finding and applying a non-stationary smoothing operator to minimize the local frequency difference between data sets. Numerical examples demonstrate that the proposed method improves multicomponent image registration and matching images of differing resolutions.

INTRODUCTION

Matching seismic data has many applications in geophysical processing methods, such as multi-component image registration, time-lapse image registration, matching well-ties to seismic data, and merging seismic data sets (????). Typically, the workflow for matching data involves finding the optimal time shift, or amount of stretching and compressing, of one trace relative to the other that produces the greatest similarity between the two traces, as seen in dynamic time warping and local similarity scanning (???). However, when the two signals that need to be aligned have different spectral content, their comparison can be difficult. Seismic data contain non-stationary, or spatially and temporally variant, frequency content caused by attenuation. This problem was discussed in application to multicomponent image registration by ?, who applied frequency balancing methods to improve registration results. ? proposed using local time-frequency decomposition (LTFD) to balance frequencies between multicomponent data during registration. However, LTFD is a relatively computationally expensive method.

In this chapter, we propose methods for removing non-stationary frequency differences that limit the effectiveness of matching data. We suggest applying either of the proposed methods to processing flows that involve matching data before attempting to find the time shift to align their signal content. To balance frequency content, we

Parts of this chapter were first published in ?, ?, and ?. This work was done under the supervision of Dr. Sergey Fomel.

use a non-stationary smoothing operator with an adjustable smoothing radius to apply to the higher frequency data set. Our first approach finds the smoothing operator directly, but it is based on the primary assumption that the data can be modeled by a summation of Ricker wavelets. Our second approach of finding the smoothing radius is based on understanding what the smoothing operator physically does, and takes the form of an optimization problem which is solved using an iterative method. We introduce these methods and apply them to examples of merging high-resolution and conventional seismic images and multicomponent image registration.

METHOD

Two signals of differing frequencies are more difficult to correlate than signals of similar frequencies. For example, Figure 5 shows two seismic images representing the same subsurface, except they have distinctly different spectral content, as shown in Figure 7a. In order to be directly comparable, these two images should have similar frequency content. Here, we look at local frequency (?), which can be thought of as a smoothed estimate of instantaneous frequency (?). Local frequency is a more geologically accurate attribute than instantaneous frequency because it honors time-frequency uncertainty and does not contain physically unrealistic negative or extremely high frequency values (?).

In order to balance local frequency content, we propose smoothing the higher frequency data using a non-stationary triangle smoothing operator with an adjustable radius. Here, the radius at each point is the number of samples in time that that specific data point is averaged over in a triangle weight.

We find the temporally and spatially variable smoothing radius to apply to the higher frequency image to balance local frequency content with the lower frequency image by taking two approaches. The first approach is finding the smoothing radius based on assumptions of what the data we are looking at can be represented by, and the second approach is based on understanding physically what non-stationary smoothing does to a data set. Both approaches work well in different situations—the first approach is less computationally expensive than the second approach, but is only applicable when the two data sets fit the assumptions that are used to calculate what the smoothing radius is. The second approach finds the smoothing radius in an iterative manner, but it manages to work well for any data set given to it.

Theoretical smoothing radius

To demonstrate the effectiveness of finding the smoothing radius using this method, we use the *Apache* seismic data sets. The two initial images are shown in Figure 1, and their frequency content are shown in Figure 2a.

To balance the non-stationary frequency variations between data sets, we use

a simple triangle smoothing operator with an adjustable radius. Here, the radius at each point is the amount of time, in seconds, that that specific data point gets averaged over in a triangle weight in the temporal direction. We specifically look at local frequency (?), which is a time-dependent frequency attribute, and can be thought of as a smoothed estimate of instantaneous frequency (?).

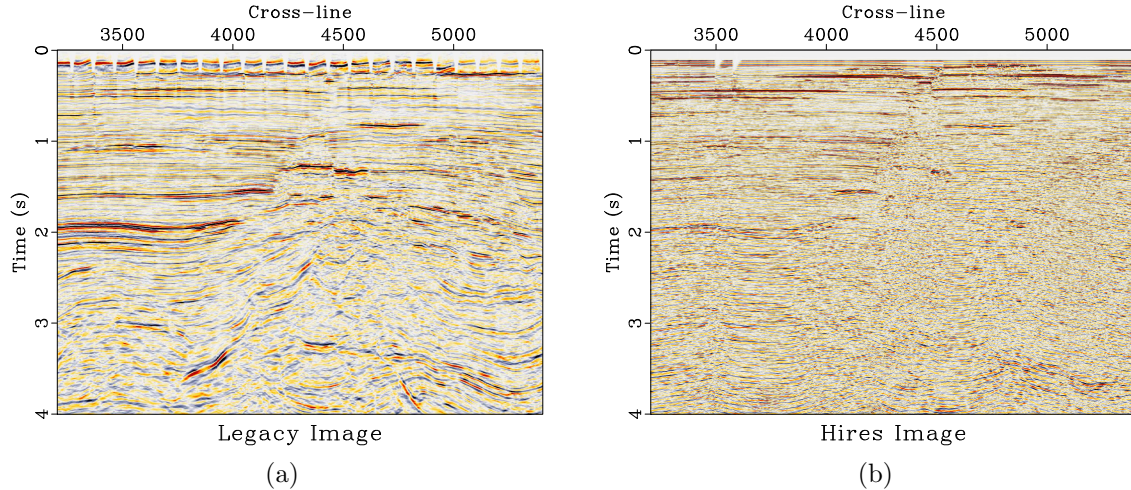


Figure 1: The initial legacy (a) and high-resolution (b) images.

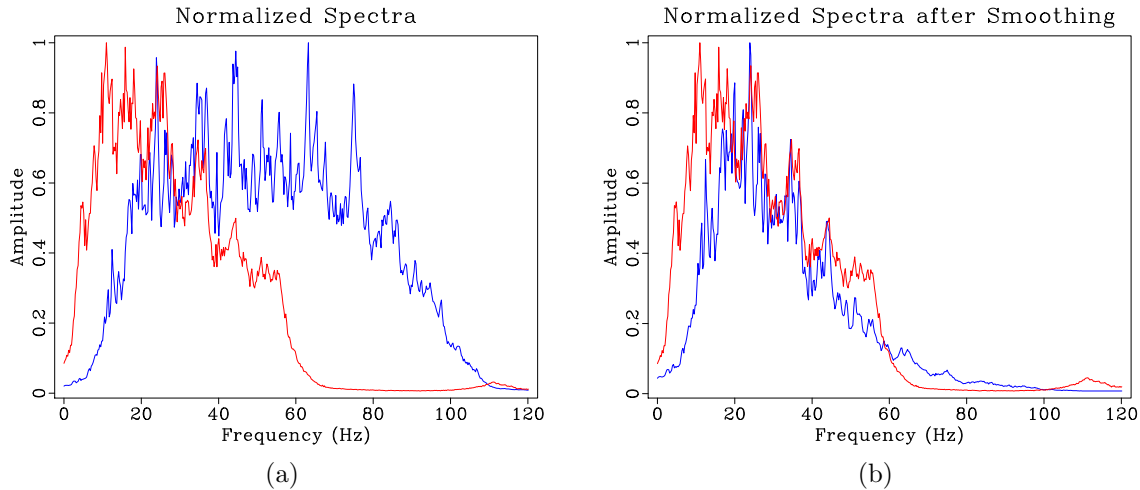


Figure 2: Spectra for the entire image display of the legacy (red) and high-resolution (blue) images before (a) and after (b) spectral balancing using the theoretical method.

This method is based off of the primary assumption that the signal can be represented by Ricker wavelets convolved with the Earth's reflectivity series. Because the data we are working with are seismic amplitudes, this can be a good assumption (?).

The justification for triangle smoothing is that it is a simple approximation to Gaussian smoothing. The frequency response of the triangle smoothing filter (?) is

$$T(f) = \text{sinc}^2\left(\frac{2\pi f \Delta t}{2}\right) \approx 1 - \frac{(2\pi f)^2 (\Delta t)^2}{12}. \quad (1)$$

This frequency response resembles that of a Gaussian:

$$G(f) = e^{-\alpha f^2} \approx 1 - \alpha f^2. \quad (2)$$

If the signals' spectra can be represented by Ricker wavelets,

$$S_n(f) = A_n \left(\frac{f}{f_n} \right)^2 e^{-\left(\frac{f}{f_n}\right)^2} \quad (3)$$

where, in image n , S_n is the frequency spectrum, f_n is the peak frequency, and A_n is the amplitude, Gaussian smoothing can transform the signal to a different dominant frequency.

Because we are smoothing the high-resolution image to match it with the legacy image, we can relate the high-resolution frequencies, S_h , to the legacy frequencies, S_l , such that

$$S_l(f) = A e^{-\alpha f^2} S_h(f) \quad (4)$$

where $A = A_l/A_h$,

$$\alpha = \frac{1}{f_l^2} - \frac{1}{f_h^2}, \quad (5)$$

and the subscripts l and h correspond to the legacy and high-resolution images, respectively.

Combining equations (1), (2), and (5) leads to the specification of the triangle smoothing radius as

$$\Delta t \approx \frac{1}{2\pi} \sqrt{12 \left(\frac{1}{f_l^2} - \frac{1}{f_h^2} \right)}. \quad (6)$$

Here, Δt is the radius of smoothing, measured in seconds, applied to the high-resolution image to match the frequency content with the legacy image at each sample. The calculated smoothing radius for this data set is shown in Figure 3.

We measure local frequencies in both images and apply smoothing specified by equation (6) to the high-resolution image. Because this is only an approximation of what the smoothing radius should be under ideal conditions, we adjust the constant 12 in the equation to achieve a better match. In this example, this effectively reduces the difference between the spectral content of the images, as shown in Figure 2b. Figure 4 shows the difference in local frequencies before and after smoothing. After smoothing, the frequency difference is minimized.

This method works well for simple data sets with overlapping frequency content. However, more complicated data sets, as seen in the next example, may require additional steps for successful frequency balancing.

Iterative method for calculating the smoothing radius

The theoretical smoothing radius works in some situations, like in the first example of the next chapter, but it does not work in situations where little overlap is present in

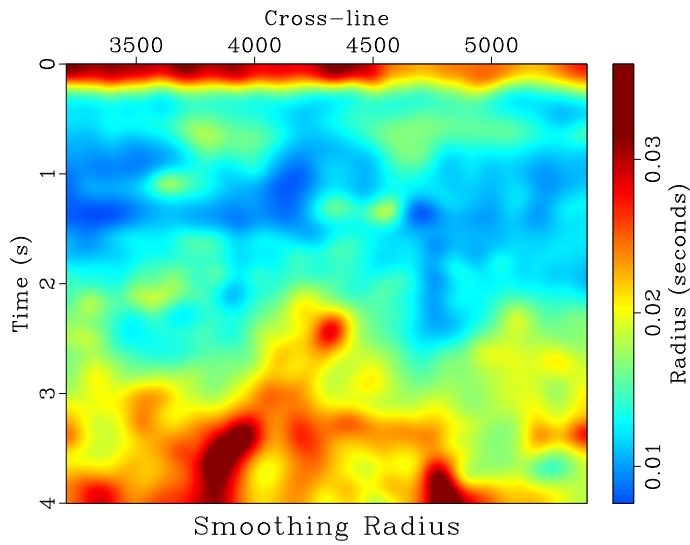


Figure 3: Calculated spatially and temporally variable smoothing radius. This represents the number of seconds in the temporal direction that the high-resolution image gets averaged over in a triangle weight to balance local frequency content with the legacy image at each sample.

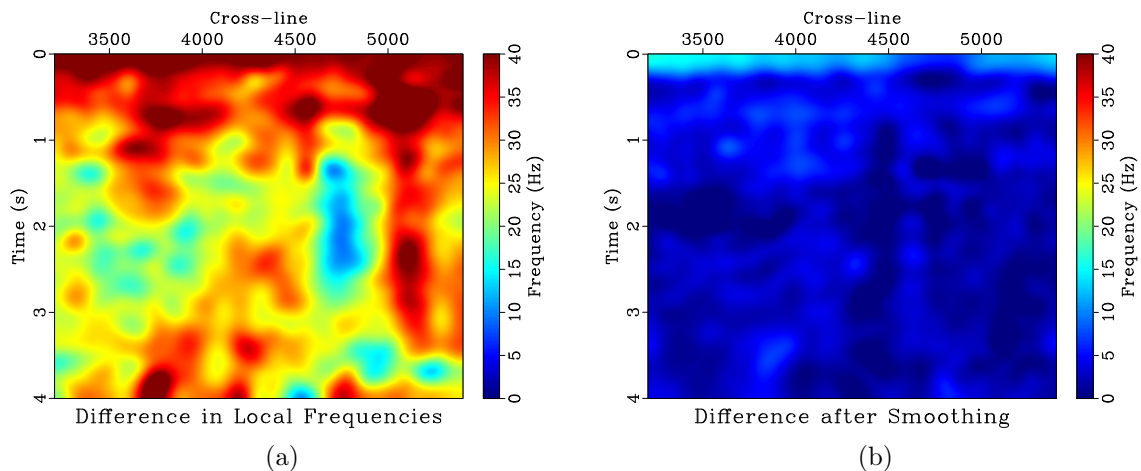


Figure 4: Difference in local frequencies between the legacy and high-resolution images before (a) and after (b) balancing their frequency content by non-stationary smoothing.

frequency content between data sets, like in the second example of the next chapter. In this case, we use an iterative method to find what the smoothing radius should be that is based on the physical understanding of what smoothing is doing.

The goal of this method is to find the temporally and spatially variable smoothing radius, \mathbf{R} , that minimizes the difference in local frequencies between the two data sets. This can be shown in the objective function

$$\min_{\mathbf{R} \in [1, N]} \left\| \mathbf{F}[\mathbf{S}_{\mathbf{R}} \mathbf{d}_h] - \mathbf{F}[\mathbf{d}_l] \right\|, \quad (7)$$

where $\mathbf{S}_{\mathbf{R}}$ is the non-stationary smoothing operator of smoothing radius \mathbf{R} , \mathbf{d}_h is the higher frequency data, \mathbf{d}_l is the lower frequency data, \mathbf{F} is the local frequency operator, and N is the maximum size of the smoothing radius. Although smoothing is a linear operation, the smoothed data, $\mathbf{S}_{\mathbf{R}} \mathbf{d}_h$, depends non-linearly on \mathbf{R} . However, the objective from equation (7) is nearly convex, and we choose to use an intuitive iterative approach to find an approximate smoothing radius.

The main premise behind the method comes from the fact that, in general, the greater the smoothing radius, the more high frequencies are attenuated by smoothing.

1. The smoothing radius is too *small* at a specified point if, after smoothing, the higher frequency data has *higher* local frequency than the lower frequency data. Thus, the smoothing radius must be *increased* at that point.
2. The smoothing radius is too *large* at a specified point if, after smoothing, the higher frequency data has *lower* local frequency than the lower frequency data. Thus, the smoothing radius must be *decreased* at that point.

We apply these assumptions using a line-search method:

$$\mathbf{R}^{(i+1)} = \mathbf{R}^{(i)} + c \mathbf{r}^{(i)}, \quad (8)$$

where $\mathbf{R}^{(i)}$ is the smoothing radius at the i th iteration, c is a scalar constant that can be thought of as the step length, and $\mathbf{r}^{(i)}$ is the residual at the i th iteration, which can be thought of as the search direction, and is defined as

$$\mathbf{r} = \mathbf{F}[\mathbf{S}_{\mathbf{R}} \mathbf{d}_h] - \mathbf{F}[\mathbf{d}_l]. \quad (9)$$

It can be noted that when equation (9) is positive, the higher frequency data still has a higher local frequency value at that specific point than the lower frequency data, thus the higher frequency data is under-smoothed and the smoothing radius should be increased at that point. This follows the form of the first assumption. The second assumption is used when equation (9) is negative. When equation (9) is zero, the correct radius has been found and no further corrections are made. Thus, it is justifiable to set the search direction from equation (8) equal to the residual.

Using the assumptions, we can choose an initial guess for the smoothing radius and continually adjust the smoothing radius until we achieve the desired result of

balancing the local frequency content between the two data sets. In practice, this method produces an acceptable solution in approximately 5 iterations and exhibits sublinear convergence. After smoothing the higher frequency data with the estimated radius, we use the lower frequency and smoothed higher frequency data to estimate time shifts and align the two data sets.

This method is applicable to workflows that require matching data with different frequency content. Here, we demonstrate that using this algorithm to match high-resolution and legacy seismic images improves the results.

High-resolution seismic data, such as those acquired with the P-cable acquisition system, can produce very detailed images of the near subsurface (?). When compared to conventional seismic images, high-resolution images have a higher dominant frequency and a wider frequency bandwidth. However, they usually lack low frequency content and depth coverage that is present in conventional seismic images. As a result, successful interpretation of high-resolution images can be aided by matching with legacy data coverage over the same area.

Example legacy and high-resolution images of the same subsurface are shown in Figure 5. The first step in matching the two images is to ensure that they both have a similar frequency bandwidth so they are directly comparable. The average frequency spectra for the two images are shown in Figure 7a. From this, it is evident that there is almost no overlap in frequency bandwidth between the two images. To address this problem, we apply a low-cut filter to the legacy image to remove some of the lower frequencies that are simply not present in the high-resolution image. Next, we implement the method described in the previous section to balance local frequency content between the two images. The difference in local frequencies (residual, by equation 9) between the high-resolution and legacy images before balancing frequency content and after 5 iterations of the algorithm in equation (8) is shown in Figure 8. After balancing local frequencies, the images show a similar spectral bandwidth (Figure 7b), which helps increase the correlation between the two images and makes matching reflections better defined.

After the frequency content is matched, the optimal time shift is found to align signal content between the legacy and high-resolution images. We then apply this time shift to the original high-resolution image—the frequency content is only degraded for the purpose of finding the time shift.

An application of aligning the high-resolution and legacy images is discussed in the next chapter.

Iterative method for calculating the smoothing radius: A modification

The algorithm previously presented works well in cases when one data set has clearly higher frequency content than the other. However, in some cases, the two data sets

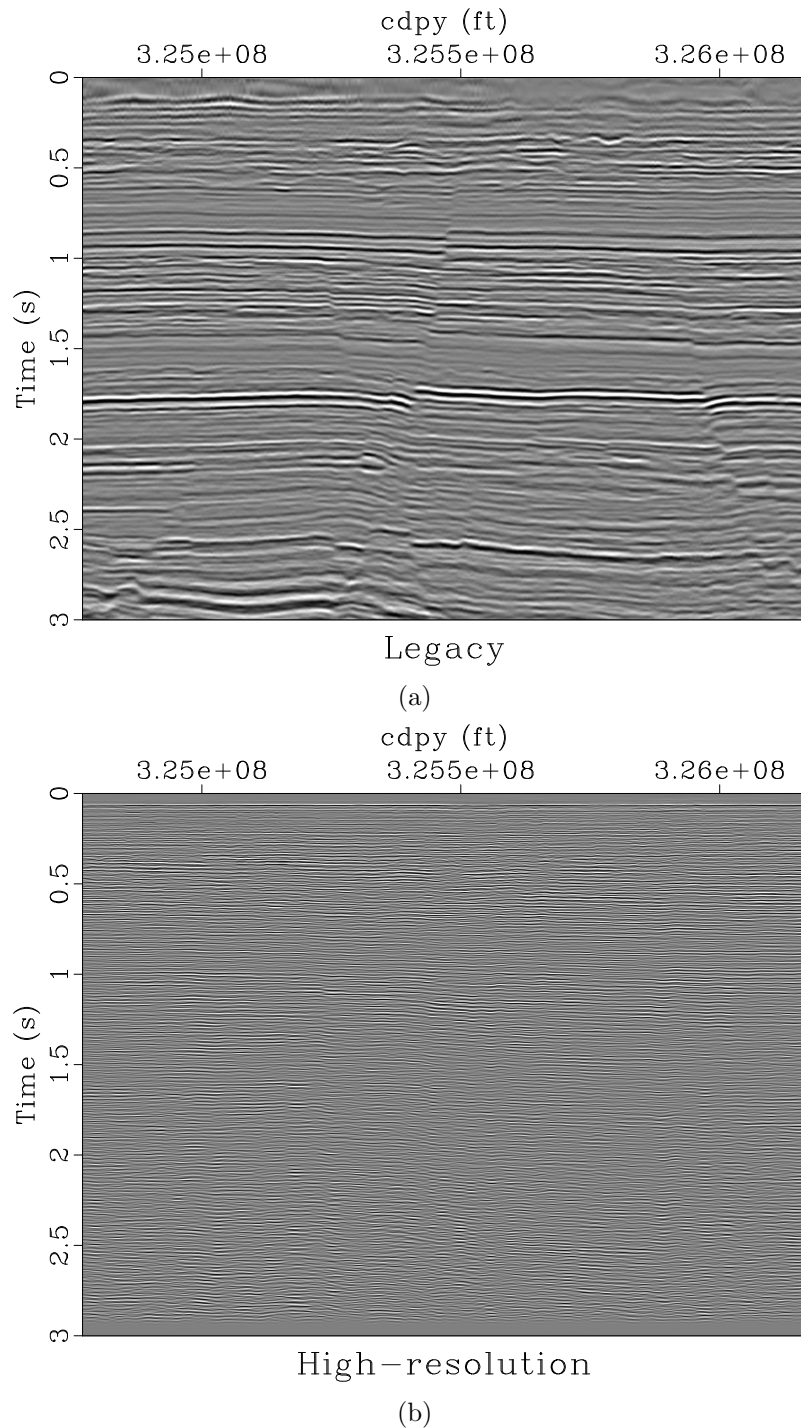


Figure 5: Initial legacy (a) and high-resolution (b) images. These images show the same subsurface geology, but look remarkably different as the high-resolution image has distinctly higher frequency content than the legacy image.

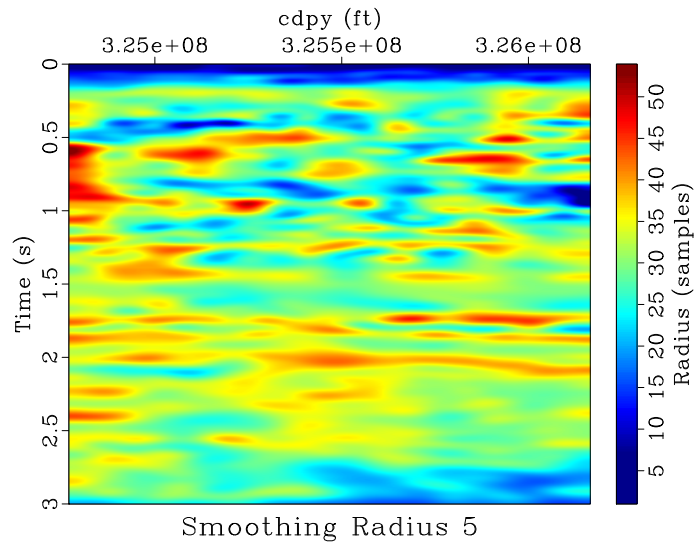


Figure 6: The smoothing radius, which is a function of time and space, this method produces after 5 iterations. This represents the number of samples in time that the high-resolution image needs to be smoothed over in a triangle weight to balance local frequency content with the legacy image.

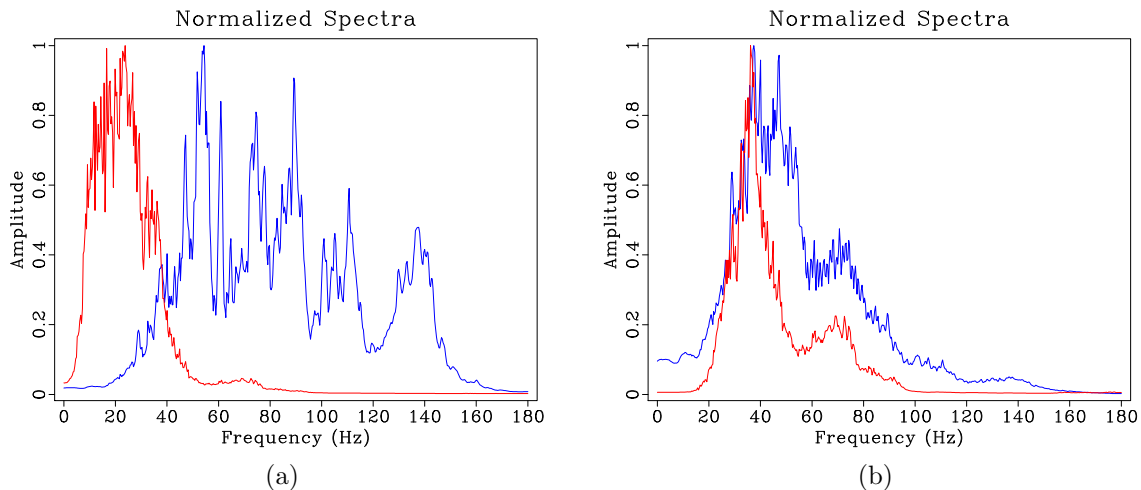


Figure 7: Spectral content of the legacy (red) and high-resolution (blue) images before (a) and after (b) spectral balancing using the theoretical method.

may have similar local frequency content, but they might still need to be matched. We illustrate a modified version of the previous algorithm by demonstrating it on an example of multi-component seismic image registration.

Multicomponent seismic image registration is an important step before the interpretation of P and S images of the subsurface. It involves warping the space of S images to align reflections with the analogous reflections of P images (??).

Figure 9 shows PP and SS images from a 9-component seismic survey (?). To properly register the images, we follow the method proposed in ?. It consists of three primary steps: (1) initial registration of PP and SS images using initial interpretation and well-log analysis; (2) balancing frequency and amplitude content; and (3) final registration using residual local similarity scanning. We incorporate our method of balancing frequency content into the second step in this process.

Before initial registration, the PP image has much higher frequency content than the SS image. After the SS image is temporally compressed to PP time for initial registration, the two images have more similar frequency content. However, additional frequency balancing is still needed before residual registration. This poses a problem as neither image has distinctly higher frequencies than the other, so both images need to be smoothed in different areas to balance frequency content. In order to do this, we modify the proposed method to include two separate smoothing operators—one for each image.

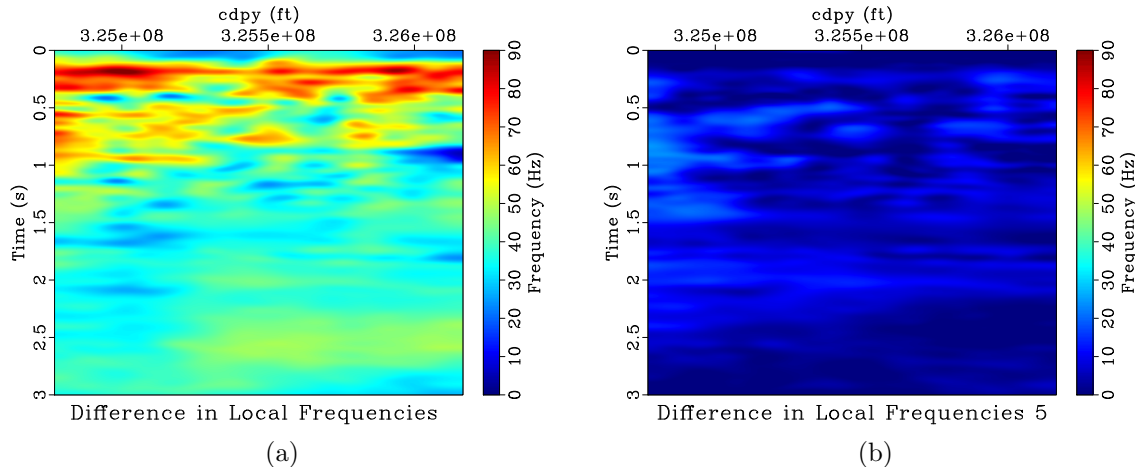


Figure 8: Difference in local frequencies (residual) between the legacy and high-resolution images before (a) and after (b) the 5th iteration of frequency balancing.

We modify the objective in equation (7) as

$$\min_{\mathbf{R} \in [-N, -1] \cup [1, N]} \left\| \mathbf{F}[\mathbf{S}_{\mathbf{R}_p} \mathbf{d}_p] - \mathbf{F}[\mathbf{S}_{\mathbf{R}_s} \mathbf{d}_s] \right\|, \quad (10)$$

where \mathbf{d}_p and \mathbf{d}_s are the PP and SS images, respectively, and $\mathbf{S}_{\mathbf{R}_p}$ and $\mathbf{S}_{\mathbf{R}_s}$ are the non-stationary smoothing operators for the PP and SS images, respectively. We also

modify the residual from equation (9) as

$$\mathbf{r} = \mathbf{F}[\mathbf{S}_{\mathbf{R}_p} \mathbf{d}_p] - \mathbf{F}[\mathbf{S}_{\mathbf{R}_s} \mathbf{d}_s]. \quad (11)$$

The ideal radius is still found using the same line-search from equation (8), except we allow the smoothing radius to be negative. Physically, a negative smoothing radius would signify that the image should be sharpened at that particular point instead of smoothed. In this case, instead of trying to sharpen the PP image at that particular point, we choose to smooth the SS image by the negative part of the smoothing radius. Thus, we define the i th components of \mathbf{R}_p and \mathbf{R}_s as

$$R_{p,i} = \begin{cases} R_i & \text{if } R_i \geq 1 \\ 1 & \text{otherwise} \end{cases} \quad (12)$$

and

$$R_{s,i} = \begin{cases} |R_i| & \text{if } R_i \leq -1 \\ 1 & \text{otherwise} \end{cases} \quad (13)$$

where R_i is the i th component of \mathbf{R} and a radius of 1 represents no smoothing. This allows each image to be smoothed in different areas to balance the frequency content between the two images.

The results of using this spectral balancing method are shown in Figure 10. Comparable results were achieved in ?, who used local time-frequency decomposition (LTFD) to balance the spectral content between the two images. However, the method we propose in this chapter is more straightforward and significantly less computationally expensive.

So far, this algorithm and its modification have been discussed when the smoothing radius is only calculated along one dimension. However, Chapter 5 provides an application where the smoothing radius is calculated in multiple directions.

CONVERGENCE ANALYSIS

Because this algorithm was developed from observations and intuition based on what smoothing is physically doing, no error analysis or convergence criteria has been developed in this thesis. However, it is observed that this algorithm generally exhibits sublinear convergence. Additionally, the initial guess for what the smoothing radius should be negligibly impacts the final result. Figure 11a shows the convergence of the algorithm from equation (8) when applied to the *P-cable* data set from the second example in this chapter (Figure 5). It is evident that no matter the initial guess, the resulting convergence is relatively unaffected, and with the correct choice of step length c , converges in few iterations. After convergence, continuing iterations do not affect the final result.

Figure 11b shows the convergence when choosing different values of c , the step length from Equation (8). From this, it is evident that the step length is important

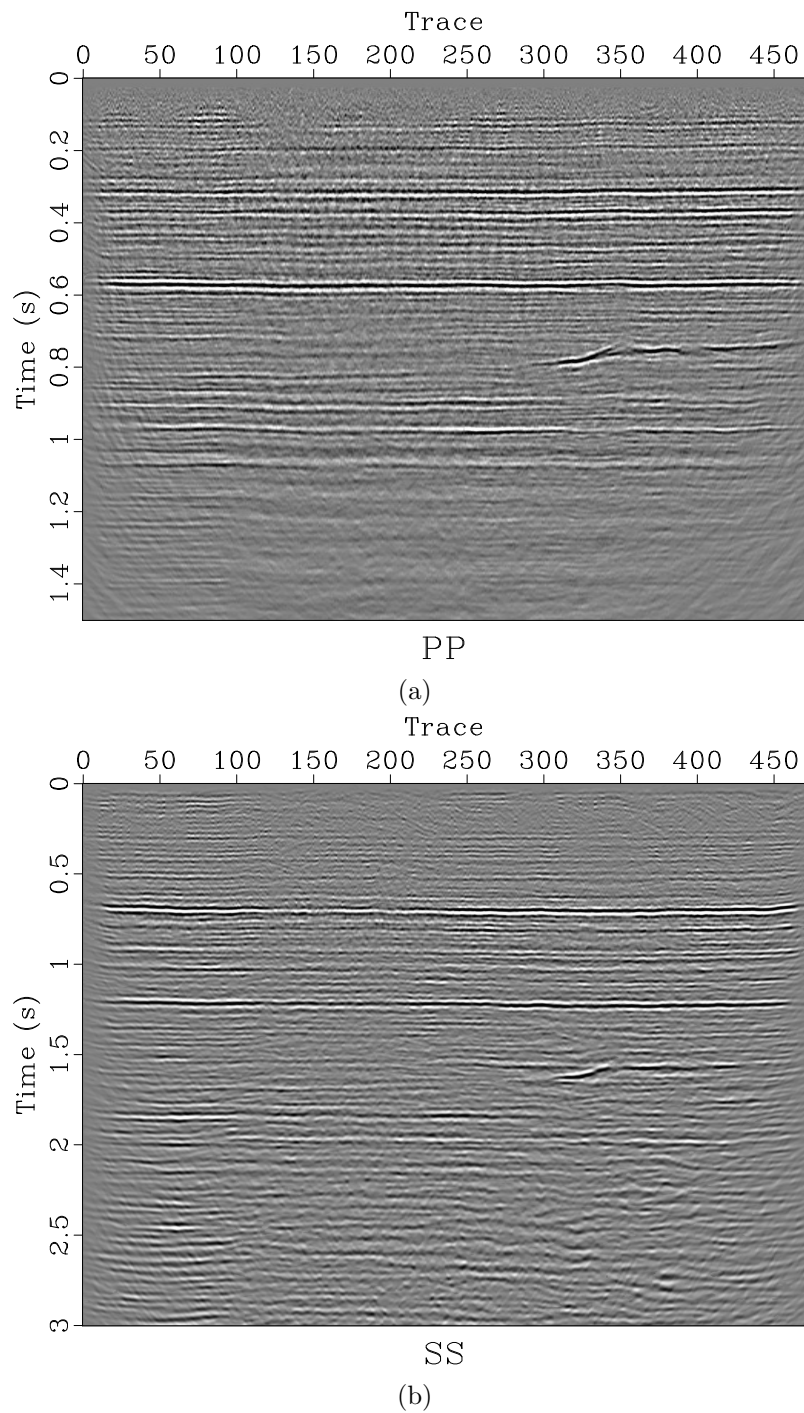


Figure 9: Initial PP (a) and SS (b) images.

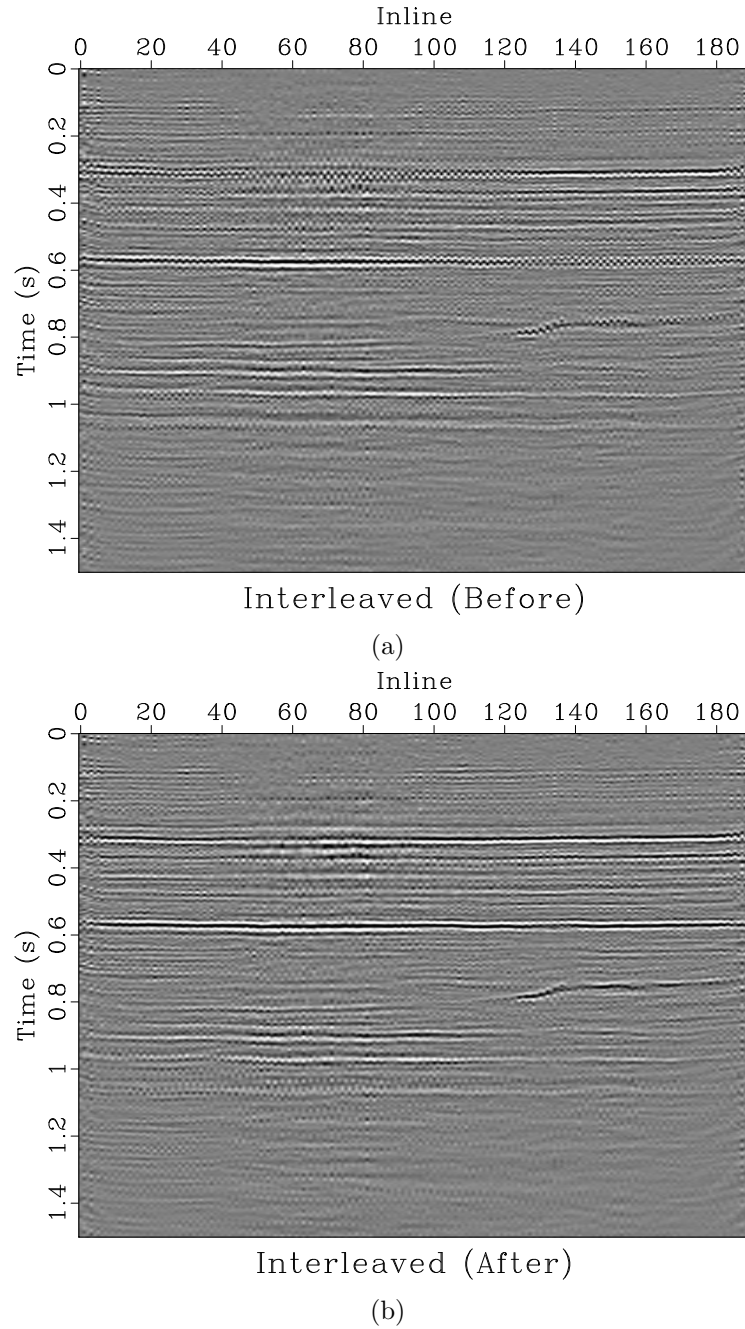


Figure 10: Interleaved PP and warped SS traces before (a) and after (b) frequency balancing and residual registration. After registration, the signal content between the two initial images is more aligned; for example, the reflections around 0.3 and 0.6 s. This indicates a successful registration.

for fast and stable convergence. If too large a step length is chosen, the method does not converge to the ideal solution. If the step length is too small, the algorithm takes many more iterations to converge. With the “correct” step length, however, the algorithm usually converges in fewer than 10 iterations in practice.

CONCLUSIONS

Comparing signals with differing frequency content is difficult because signals with differing frequencies are hard to correlate. In this chapter, we proposed two methods of balancing frequency content between data. The first one takes a theoretical approach of what we expect the data to be, and the second one takes the form of an optimization problem solved by a simple iterative algorithm. This algorithm is a relatively inexpensive and effective method compared to previously proposed methods of balancing frequencies between data sets. We applied these methods to examples of matching seismic images of differing resolution and for multicomponent image registration.

ACKNOWLEDGEMENTS

We thank the sponsors of the Texas Consortium for Computational Seismology (TCCS) for their financial support.

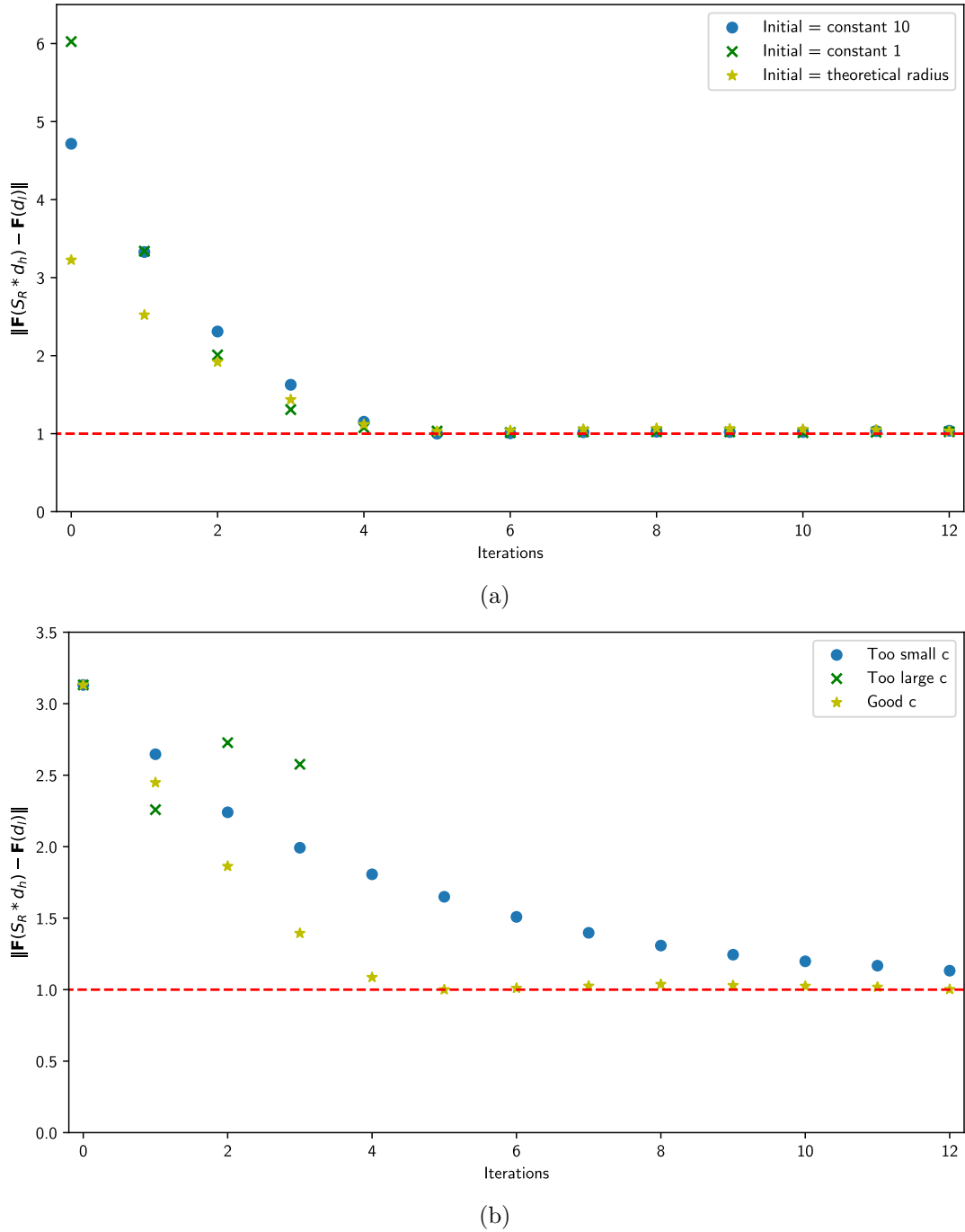


Figure 11: Convergence of the algorithm from Equation (8) for (a) different initial guesses, and (b) different choices of c , the step length, using the theoretical radius as the initial guess.